Improved carrier phase recovery for high-capacity optical communication systems with high-order modulation formats

Yunfan Zhang [a], Tiegen Liu [a], Cenqin Jin [b], Tongyang Xu [c,d], Mingming Tan [e], Jian Zhao [a,*], Tianhua Xu [a,b,c,**]

[a] School of Precision Instruments and Opto-Electronics Engineering, Tianjin University, Tianjin 300072, China
[b] School of Engineering, University of Warwick, Coventry CV4 7AL, United Kingdom
[c] Department of Electronic and Electrical Engineering, University College London, London WC1E 6BT, United Kingdom
[d] School of Engineering, Newcastle University, Newcastle upon Tyne, NE1 7RU, United Kingdom
[e] Aston Institute of Photonic Technologies, Aston University, Birmingham B4 7ET, United Kingdom

ARTICLE INFO

ABSTRACT

A modified Viterbi-Viterbi (MVV) carrier phase recovery (CPR) algorithm is comprehensively studied based on the quadrature phase-shift-keying (QPSK) partition scheme. By improving the QPSK partition scheme for the 16-ary quadrature amplitude modulation (16QAM), MVV algorithm is developed for the optical fiber communication systems with the modulation formats of dual-polarization 64-QAM (DP-64QAM) and DP-256QAM. Numerical simulations have been carried out in a 9-channel Nyquist-spaced 32-Gbaud optical transmission system for different modulation formats and the performance of MVV CPR with respect to pilot-aided (PA) CPR has been examined. Results show that MVV CPR can significantly mitigate the laser phase noise in the system using high-order modulation formats. Compared to PA CPR, MVV CPR performs better with the increase of the transmission distance, where the impact of equalization enhanced phase noise has to be taken into account. Furthermore, MVV has been compared with other CPR approaches in terms of the performance and the computational complexity.

1. Introduction

Nowadays the research on coherent optical communications has become more and more prominent because of the increasing demand for long transmission distance, large capacity, and high spectral efficiency [1–3]. In general, we can evaluate the highest achievable spectral efficiency under certain transmission scenarios according to the Shannon-Hartley theorem [4], i.e., the Shannon limit. Without increasing the symbol rate or expanding the bandwidth, the spectral efficiency can be pushed towards the Shannon limit by increasing the order of the M-ary quadrature amplitude modulation (QAM) format. Nevertheless, the laser phase noise and the equalization enhanced phase noise (EEPN) are severe limiting factors in the coherent optical communication systems, especially for the systems using high-order modulation formats [5–9]. As a result, research works on the carrier phase recovery (CPR) for systems using the high-order modulation formats are of practical significance [10,11].

Motivated by these requirements, the unprecedented development has been achieved in the area of digital signal processing (DSP) technologies, and varieties of algorithms have emerged [12], e.g. Viterbi-Viterbi (VV) [13–15], blind phase search (BPS) [16–20], quadrature phase-shift-keying (QPSK) partitioning [21,22], low-complexity constellation classification [23], multiple-input multiple-output (MIMO) CPR [24], master–slave CPR [25], modified QPSK partitioning [26], rotation algorithm (RA) [27], constellation transformation (CT) algorithm [28,29], pilot-aided (PA) CPR [30–41] and so on. In addition to these classic approaches, there are also several newly-developed algorithms, including dichotomy blind phase search (DBPS) [42], linewidth-tolerant multi-format carrier phase estimation [43], enhanced adaptive decision-aided maximum likelihood (DA-ML) carrier phase estimator [44], transmission-aware carrier phase estimation [45] and so on.

In this paper, a modified Viterbi-Viterbi (MVV) CPR algorithm for the DP-64QAM and the DP-256QAM optical communication systems has been developed, in order to verify the feasibility of upgrading the

---

* Corresponding author.
** Corresponding author at: School of Engineering, University of Warwick, Coventry CV4 7AL, United Kingdom.
E-mail addresses: enzhaojian@tju.edu.cn (J. Zhao), tianhua.xu@ieee.org (T. Xu).
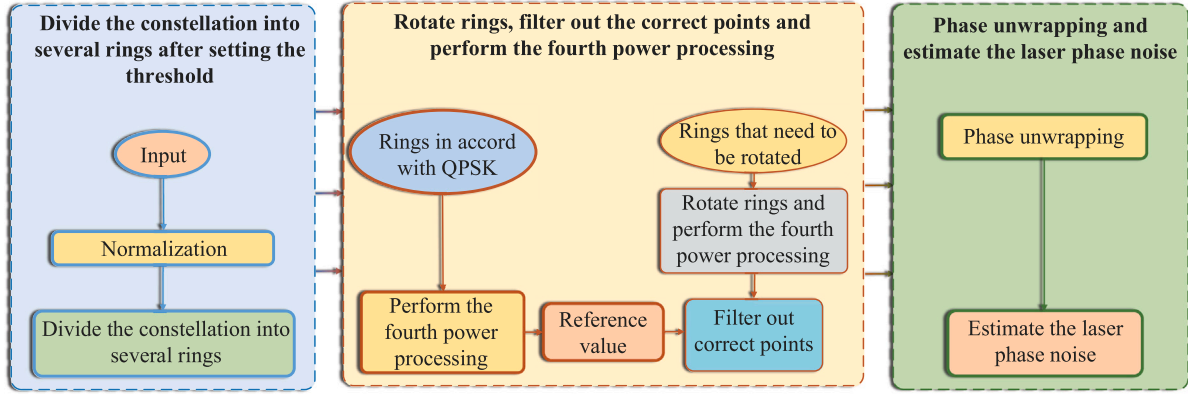
Fig. 1. Principle of the modified Viterbi-Viterbi algorithm.

current DP-16QAM 200 Gbit/s/λ transmission schemes. Initial research has been carried out in our previous work where the performance of MVV CPR was examined in a linear optical communication system [46]. While in this paper, we have investigated more practical cases and provided more comprehensive analyses, when Kerr fiber nonlinearities are taken into account, to study the performance of MVV CPR in more realistic transmission scenarios. A 9-channel, 32-Gbaud Nyquist-spaced wavelength division multiplexing (WDM) optical communication system is implemented to study the performance of MVV CPR. Numerical simulations indicate that MVV CPR not only can greatly compensate for the laser phase noise but also can significantly reduce the effect of EEPN. The application of MVV CPR is also studied in the DP-256QAM optical system, to demonstrate its capability for further higher-order modulation formats. Furthermore, MVV is also compared with other classic CPR algorithms in terms of the performance and the computational complexity.

2. Principle of MVV CPR

2.1. Laser phase noise model

The laser phase noise is generally modeled as a Wiener process [47], which can be described as [48,49]

$$\varphi_t = \sum_{i=-\infty}^{t} N_i \tag{1}$$

where N_i is an independent and identically distributed random Gaussian variable, of which the variance can be described as

$$\sigma_f^2 = \frac{2\pi \Delta v}{R_s} = 2\pi(\Delta v T_s) \tag{2}$$

where Δv represents the linewidth, R_s denotes the symbol rate, and T_s represents the symbol period. As Eq. (2) reveals, the laser phase noise variance increases with the 3-dB linewidth of the laser and the symbol period of the transmission system.

2.2. Principle of MVV CPR

The QPSK partition scheme improves Viterbi-Viterbi algorithm for the 16QAM modulation format [5,42,50–57]. In this work, we have further improved the QPSK partition scheme for the 64QAM modulation format. The core idea of the algorithm is to make all symbol points, within a sliding window, conform to the QPSK modulation format through a series of rotations so that all constellation points can be used to estimate and remove the laser phase noise [43,58–61]. The principle of the MVV algorithm is illustrated in Fig. 1.
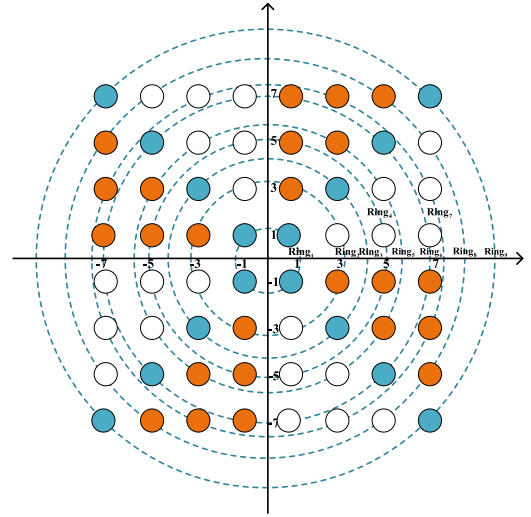

Fig. 2. Rotation operation on the 64QAM constellation. There are 64 colored circles in the coordinate system, and each of them represents one symbol point in the 64-ary constellation. From the figure, we could see that blue points could be treated as standard QPSK constellation points. Both orange points, after a few clockwise rotations, and white points, after a few anti-clockwise rotations, can also be treated as standard QPSK constellation points. Consequently, all points can conform to standard QPSK constellation points after certain rotation operations.

1. Divide the constellation into nine rings after setting amplitude thresholds
   Firstly, perform the normalization on the input symbol sequence to make their amplitude consistent with the coordinate system in Fig. 2. In this coordinate system, radii of the nine rings are $\sqrt{2}$, $\sqrt{10}$, $3\sqrt{2}$, $\sqrt{26}$, $\sqrt{34}$, $5\sqrt{2}$, $\sqrt{58}$, $\sqrt{74}$, and $7\sqrt{2}$, respectively. The first step is to classify all received symbols into these nine rings by comparing the magnitude of each symbol with eight thresholds derived from the radii of the nine rings. Here we set each threshold to be half of the sum of two adjacent rings. For example, in the coordinate system shown in Fig. 2, the first threshold can be set as follows:

$$Thr_1 = (\sqrt{2} + \sqrt{10})/2 \tag{3}$$

2. Perform the fourth power operations, rotations and filtering out operations
   After comparing the amplitude of each symbol with all thresholds, all symbol points can be classified into nine rings. Obviously, for the symbols in the $Ring_1$, $Ring_3$, and $Ring_9$, the fourth power operation can be directly applied to remove the data modulation. Although symbols at other rings cannot be

processed with the fourth power operations directly, they can be regarded as several sets of QPSK signals with different rotations against the symbols in the $Ring_1$, $Ring_3$, and $Ring_9$.

In MVV CPR, the constellation points can be divided into subgroups of QPSK signal points, i.e., blue points, white points, and orange points, which are denoted respectively as X_{QPSK}, X_w, and X_o, as illustrated in Fig. 2. Blue points, X_{QPSK}, can be processed directly by performing the fourth power operations. For each ring, the white symbols and orange symbols, namely X_w, and X_o, correspond to two different sets of QPSK points with phase offsets $\pm\theta_n$ with respect to X_{QPSK} points on the same ring, as shown in Fig. 2. For $Ring_2$, $Ring_4$, $Ring_5$, $Ring_6$, $Ring_7$, and $Ring_8$, the corresponding θ_ns are $angle(1+3i)-\pi/4$, $angle(1+5i)-\pi/4$, $angle(3+5i)-\pi/4$, $angle(1+7i)-\pi/4$, $angle(3+7i)-\pi/4$, and $angle(5+7i)-\pi/4$, respectively. For example, the set of points in the $Ring_2$, i.e., X_w and X_o, can be rotated by either $angle(1+3i)-\pi/4$ or $\pi/4-angle(1+3i)$ to remove the phase modulation when performing the fourth power operations. Note that blue points in $Ring_6$ are not included in X_{QPSK}, since there are both blue and white points in $Ring_6$.

Therefore, after being normalized, X_{QPSK} are raised to the fourth power to remove the phase modulation, while X_w and X_o are rotated by $+\theta_n$ and $-\theta_n$ to consider both rotation possibilities, because it is difficult to judge which subgroup the considered symbol point belongs to. Each rotated pair is then raised to the fourth power $\{(X_{w,o}^+)^4, (X_{w,o}^-)^4\}$ to remove the phase modulation with the correct but yet unknown orientation. This will lead to two possible cases: a wrong estimate due to the incorrect rotation and a correct estimate close to X_{QPSK} within the sliding window. This is because the laser phase changes continuously within the CPR window in the high-speed optical communication system (very short symbol period). Therefore, X_{QPSK} could be used as a reference to judge the correct rotation from the pair $\{(X_{w,o}^+)^4, (X_{w,o}^-)^4\}$.

All $(X_{QPSK})^4$ symbols within the CPR window are summed up and normalized:

$$\overline{X_{QPSK}} = \frac{1}{k}\left[\sum_k (X_{QPSK})^4\right] \qquad (4)$$

where the value of k depends on the number of $(X_{QPSK})^4$ in the CPR window. The mean of the estimate $\overline{X_{QPSK}}$ is also normalized similarly as the other symbols within the CPR window. Since the laser phase changes continuously and the symbol period is very small, it is reasonable to use $\overline{X_{QPSK}}$ as a reference to select correct symbol points from the pair $\{(X_{w,o}^+)^4, (X_{w,o}^-)^4\}$ (within each CPR window) by comparing the modulus of the complex difference between $(X_{w,o}^+)^4/(X_{w,o}^-)^4$ and $\overline{X_{QPSK}}$ with the threshold Thr_{fil}, after the normalization of $(X_{w,o}^+)^4/(X_{w,o}^-)^4$. Note that for $Ring_6$, the pair is $\{(X_{w,o}^+)^4, (X_{w,o}^-)^4, (X_0)^4\}$, where X_0 represents the blue points in $Ring_6$. If the modulus of the complex difference is smaller than the threshold, the rotated symbols of $(X_{w,o}^+)^4/(X_{w,o}^-)^4$ are considered to be close enough to $\overline{X_{QPSK}}$. This means that such symbol points have been processed with correct rotations.

$$Y(n)^4 = \frac{1}{2}\{X(n)_{pair}^4 \cdot \{1 - sgn[Mod(X(n)_{pair}^4$$
$$- \overline{X_{QPSK}}) - Thr_{fil}]\}\} \qquad (5)$$

where $Y(n)^4$ represents the symbol point after the proper rotation, originating from $X(n)_{pair}^4$. $X(n)_{pair}^4$ represents the considered symbol point in the symbol sequence of the pair $(X_{w,o}^+)^4/(X_{w,o}^-)^4$, $sgn(\cdot)$ is the $signum$ function, and $Mod(\cdot)$ is the $modulus$ function which returns the modulus of the input complex number. After the above operations, the modulation information in all symbol points are removed. In addition, the random phase fluctuations created by AWGN sources (e.g. ASE noise from optical amplifiers

Table 1
Transmission system parameters.

Parameter	Value
Symbol rate	32 Gbaud
Channel spacing	32 GHz
Central wavelength (both transmitter and LO)	1550 nm
Number of channels	9
Roll-off	0.1%
Attenuation coefficient (α)	0.2 dB/km
Chromatic dispersion coefficient (D)	17 ps/nm/km
Nonlinear coefficient (γ)	1.2 /W/km
Span length	80 km
EDFA noise figure	4.5 dB

and EEPN) need to be suppressed as much as possible before we estimate the laser phase noise. In MVV CPR, a scheme of the sliding window averaging [21,62] is introduced. Summing up and averaging $Y(n)^4$ within each CPR sliding window can effectively mitigate the random phase fluctuations created by AWGN sources [63]. After these steps, the estimated laser phase noise in each symbol can be described as:

$$\phi(n) = \frac{1}{4}angle\left\{\sum_{k=-N}^{k=N} Y(n+k)^4\right\} \qquad (6)$$

where $\phi(n)$ represents the estimated laser phase noise in the nth symbol, and the length of the sliding window is $2N+1$.

3. Phase unwrapping and the laser phase noise estimate
Generally, the range of the output in the angle function is $[-\pi, \pi]$, and thus the range of the estimated laser phase noise according to Eq. (6) is $[-\pi/4, \pi/4]$. When the actual value of the laser phase noise exceeds this range, the effect of the cycle slip will occur and this will bring additional errors [64,65]. Therefore, it is necessary to unwrap the estimated laser phase fluctuation to avoid the phase ambiguity [66]. After the phase unwrapping, the correct estimation of the laser phase noise can be obtained.

3. Transmission setup

Fig. 3 illustrates the transmission setup of the 9-channel 32-Gbaud Nyquist-spaced wavelength division multiplexing (WDM) optical communication system. Detailed parameters of the transmission system are shown in Table 1. At the transmitter, we use a 32-GHz spaced laser comb with a central wavelength of 1550 nm to produce the optical carriers. Subsequently, the WDM optical carriers are modulated by 32-Gbaud signals via in-phase and quadrature (I-Q) modulators, respectively, and the transmitted symbol sequences in each channel are random and independent.

In the transmission link, the standard single-mode fiber (SSMF) is simulated based on the split-step Fourier solution of the nonlinear Schrödinger equation (NLSE), with a logarithmic distribution of the step size. At the receiver, the signals are split into two orthogonally-polarized branches by the polarization beam splitter (PBS), then they are mixed with the LO laser carrier to implement the coherent detection. The signals are further sampled by the analog-to-digital converters (ADCs) with a sampling rate of 2 samples/symbol. In the DSP module, after the compensation of chromatic dispersion [67], the CPR module is applied to mitigate the laser phase noise generated from the transmitter and the LO lasers. At the last stage, the bit-error-rate (BER) is evaluated to assess the CPR performance. The frequency offset and the polarization mode dispersion (PMD) are neglected in all simulations if not specified.

4. Results and analysis

To evaluate the developed MVV CPR, numerical simulations have been carried out in the 9-channel 32-Gbaud Nyquist-spaced optical
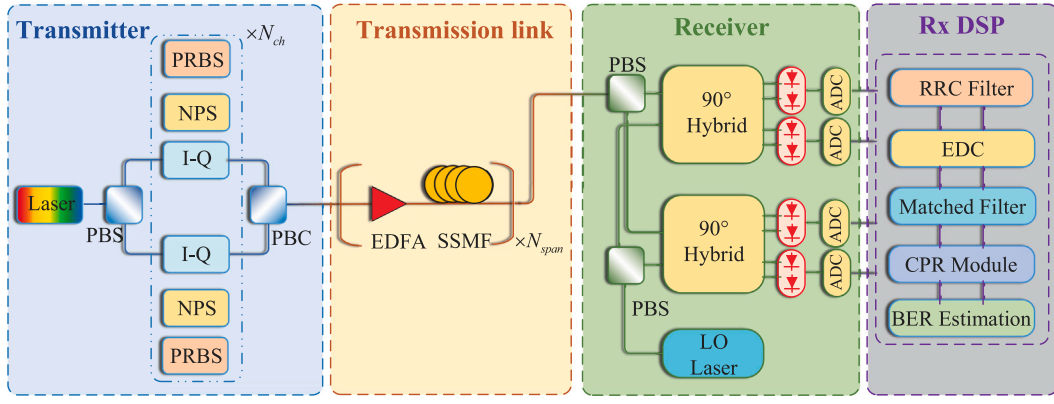
Fig. 3. Schematic of 9-channel 32-Gbaud Nyquist-spaced wavelength division multiplexing optical communication system. PRBS: pseudo-random binary sequence; NPS: Nyquist pulse shaping; PBS: polarization beam splitter; PBC: polarization beam combiner; N_{ch}: number of channels; N_{span}: number of spans; LO: local oscillator; ADC: analogue to digital converter. At the receiver, signals are sampled at 2 samples per symbol by ADCs before DSP modules.
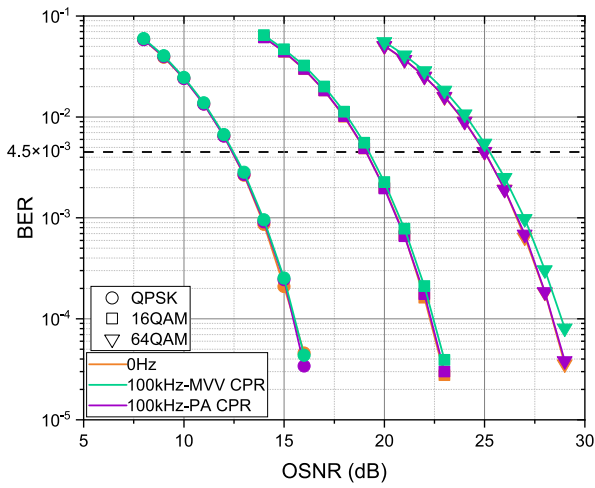

Fig. 4. BER versus OSNR in the back-to-back transmission system of Fig. 3 for different modulation formats. Three different modulation cases are considered. For each modulation format we use 0 Hz case as a reference, and compare the performance of pilot-aided (PA) CPR and MVV CPR. The length of transmitted symbol sequence is 2^{18}. OSNR: optical signal-to-noise ratio.

Fig. 5. Simulated curves of BER versus optical launch power in the transmission system of Fig. 3 for DP-64QAM over a 400 km fiber link. Three different scenarios are illustrated, and the 0 Hz case is used as a reference. The length of transmitted symbol sequence is 2^{18}.

transmission system. In all simulations, the linewidth of the transmitter laser is set equal to the linewidth of the LO laser. Besides, if not otherwise specified, the value of CPR length is always set as 61 in the following simulations.

PA CPR has been widely applied to fully compensate for the laser phase noise in the optical transmission systems, where a pilot carrier is produced to record the laser phase from the transmitter and the LO lasers [30–35]. In our simulations, we have recorded the pilot carrier from the transmitter and LO lasers to perform the same compensation effects, and the practical implementations can be realized as described in [30,31]. Since the PA CPR can fully remove the intrinsic laser phase noise, it has been widely employed as a reference to study the capability of MVV CPR in mitigating the influence of laser phase noise [68–70].

At first, we carried out a simulation in the 9-channel 32-Gbaud back-to-back transmission system. Fig. 4 provides the performance of BER versus optical signal noise ratio (OSNR) under different modulation formats, with the application of MVV CPR and PA CPR. Orange, green, and purple curves represent simulation results generated at 0 Hz linewidth, 100 kHz linewidth with MVV CPR, and 100 kHz linewidth with PA CPR, respectively. Circle, square, and triangular points represent three different modulation formats: DP-QPSK, DP-16QAM, and DP-64QAM, respectively.
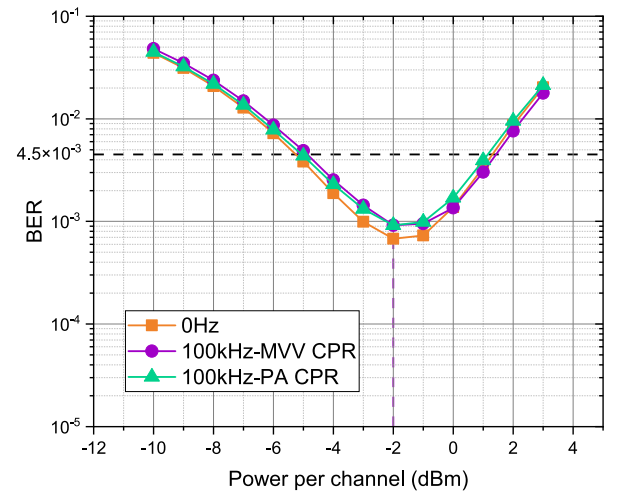
From Fig. 4 it is seen that both MVV CPR and PA CPR can significantly mitigate the impact of the laser phase noise, and MVV CPR behaves similarly as the PA CPR at all considered OSNR values. This because in the back-to-back system with the linewidths of 0 Hz and 100 kHz, there is no EEPN and the influence of the laser phase noise is also limited. Besides, the averaging function in the sliding window of MVV CPR can help mitigate the random phase fluctuations created by AWGN sources (e.g. ASE noise in the back-to-back case) [71,72].

Simulation results of BER versus optical launch power over a 400 km fiber link with the modulation format of DP-64QAM are illustrated in Fig. 5. Orange, green, and purple curves represent simulation results generated in 0 Hz transmission system, 100 kHz transmission system using PA CPR, 100 kHz transmission system using MVV CPR, respectively. As shown in Fig. 5, MVV CPR could effectively mitigate the laser phase noise for the DP-64QAM transmission system. It is found that the green curve (the performance of MVV CPR) and the purple curve (the performance of PA CPR) almost coincide. When the transmitted signal power is higher than the optimal power, the performance of MVV CPR is even slightly better than that of PA CPR. Besides, it can be seen from Fig. 5 that for MVV CPR the optimal signal power is −2 dBm per channel. In the following, all simulations are carried out at this optimal power.
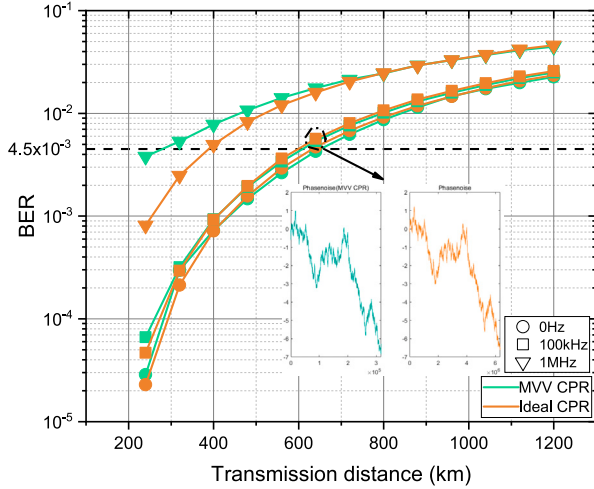
Fig. 6. BER versus optical transmission distance in the system of Fig. 3 with DP-64QAM at three different linewidths: 0 Hz, 100 kHz, and 1 MHz. For each linewidth, the performance of PA CPR and MVV CPR are compared. The length of transmitted symbol sequence is 2^{18}.

Fig. 7. BER versus linewidth in the transmission system of Fig. 3 for DP-64QAM. Results were achieved for a transmission distance of 400 km. From 100 kHz to 1.8 MHz the performance of PA CPR and MVV CPR are compared. The length of transmitted symbol sequence is 2^{18}.

In the optical transmission system shown in Fig. 3, there is a complicated interplay between the chromatic dispersion compensation and the laser phase noise in the EDC module. This interaction leads to the EEPN. The LO laser will contribute to the generation of the EEPN in the scheme of CD post-compensation, with the EEPN variance described as [5,73–78]

$$\sigma^2_{EEPN} = \frac{\pi\lambda^2}{2c} \cdot \frac{D \cdot L \cdot \Delta f_{LO}}{T_s} \tag{7}$$

where λ is the central wavelength of the optical carrier wave, c is the light speed in the vacuum, D is the chromatic dispersion coefficient of the transmission fiber, L is the transmission fiber length, Δf_{LO} is the 3-dB linewidth of the LO laser and T_s is the symbol period of the transmission system. The EEPN, i.e. the interaction between LO phase noise and electronic CD compensation, will induce additional phase distortions and amplitude distortions [75]. Since the reduction of EEPN effect is of obvious importance to improve the performance of optical transmission systems [75–78], the performance of MVV CPR is analyzed in the long-haul optical fiber communication systems, where the influence of EEPN is significant. It is noted that PA CPR is only capable of mitigating the intrinsic laser phase noise, which means that the application of PA CPR will not touch any effects of EEPN [32,34]. Therefore, PA CPR has been widely applied as a Ref. [68–70].

In addition, simulation results of BER versus transmission distance using MVV CPR are illustrated in Fig. 6, as shown with green curves. As a reference, PA CPR is used to suppress the laser phase noise and results are illustrated with orange curves. Circle, square, and triangular points represent three different scenarios: 0 Hz, 100 kHz, and 1 MHz, respectively. The inset in Fig. 6 shows the recorded (in PA CPR) and the tracked (in MVV CPR) phase fluctuations, respectively, when PA CPR and MVV CPR provide the same performance. For the same transmission distance, the performance gap between MVV CPR and PA CPR gradually increases with the increment of the laser linewidth. Nevertheless, as illustrated in Fig. 6, the performance of MVV CPR gradually approaches the performance of PA CPR, as the transmission distance becomes longer. When the transmission distance exceeds 800 km, MVV CPR behaves almost the same as PA CPR.

According to the above analyses, this is because MVV CPR can reduce the random phase fluctuations created by AWGN sources, e.g. the EEPN and the ASE noise, to a certain extent, due to the averaging function in the sliding window.
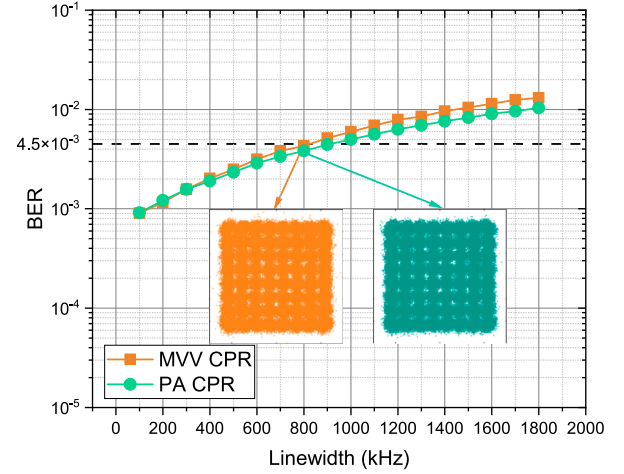
From the analyses in Section 2.2 it is obvious that the amplitude noise could be suppressed to a certain degree by applying MVV CPR due to the averaging operation within the CPR window. As the transmission distance increases, the ASE noise and the EEPN become severer. This explains the phenomenon that the performance of MVV CPR gradually approaches that of PA CPR.

Currently, the linewidth of a classical micro-integrable tunable laser is 100 kHz [79]. For linewidth of 100 kHz, it is found that the maximum reach of the transmission system in Fig. 3 using MVV CPR is 600 km at the target BER of 4.5×10^{-3}, corresponding to the 7% overhead hard-decision forward-error-correction (FEC) threshold [80].

Results of MVV CPR in the DP-64QAM system over a 400 km optical link with different linewidths are illustrated in Fig. 7, as shown with green curves. As a reference, PA CPR is used to estimate the laser phase noise and the results are illustrated with orange curves. At the target BER of 4.5×10^{-3}, the constellation diagrams of the signal processed by PA CPR and MVV CPR are shown in the inset, with green and orange points, respectively. From the results, we can see that compared with PA CPR, MVV CPR could still effectively mitigate the laser phase noise as the linewidth increases considerably. Up to now, the 3-dB linewidth of the state-of-the-art narrow-linewidth laser could be less than 1 kHz [81]. It is found that, at the target BER of 4.5×10^{-3}, the maximum tolerable linewidth of the transmission setup in Fig. 3 is 800 kHz. This indicates that MVV CPR has a strong tolerance to the laser fabrication.

Simulations have been carried out to further evaluate the influence of CPR length on the performance of MVV CPR, and results are shown in Fig. 8. Green, orange, and purple curves represent simulation results produced at linewidths of 100 kHz, 500 kHz, and 1 MHz, respectively. The optimal CPR lengths for different linewidths are highlighted with dashed lines. It can be observed in Fig. 8 that the variation of BER is faint when the CPR length varies. Over a considerable change in the CPR length, the BER does not vary much. This indicates that MVV CPR possesses the high stability. Moreover, from Section 2.2 we can draw a conclusion that there exists a trade-off between the compensation of the laser phase noise and the mitigation of random phase fluctuations created by AWGN when the CPR length is changed. The optimal CPR length varies with the value of the laser linewidth. Generally, for the system with a larger linewidth, it would be better to apply a smaller CPR length to achieve the target BER.

In addition, the performance of MVV is also investigated, when the considerable nonlinear phase noise (NLPN) exists in the DP-64QAM
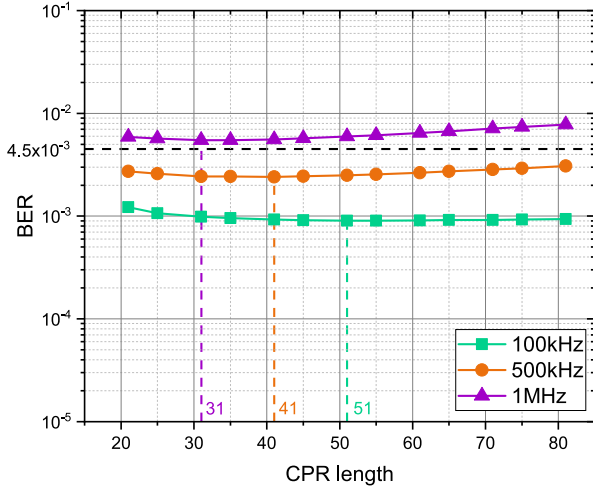
Fig. 8. Simulated curves of BER versus CPR length in the transmission system of Fig. 3 with DP-64QAM and a transmission distance of 400 km. Three different linewidths using MVV CPR are considered. The length of transmitted symbol sequence is 2^{18}.
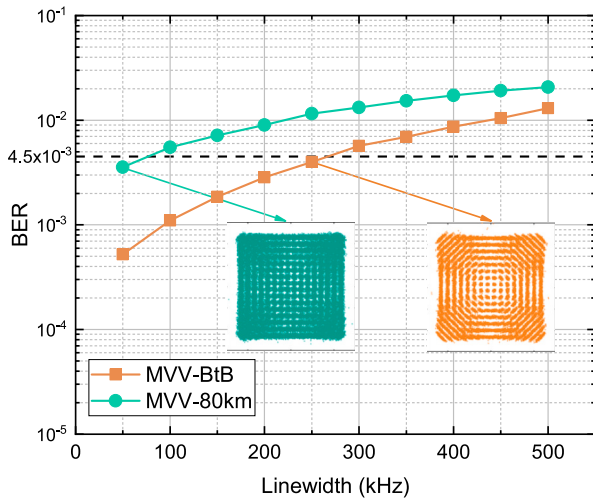

Fig. 9. BER versus laser linewidth in the transmission setup of Fig. 3 with DP-256QAM and the application of MVV CPR. Results are obtained for a back-to-back system and a transmission distance of 80 km. The performance of MVV CPR is tested with the laser linewidth of from 50 kHz to 500 kHz. The length of transmitted symbol sequence is 2^{18}.

system. The nonlinear phase noise originates from the Kerr effect in the optical fiber communication system, when it is operated with relatively high signal power and low chromatic dispersion [82,83]. Initial simulations have been carried out in a 9-channel DP-64QAM optical transmission system with a linewidth of 0 kHz (to remove the impact of laser phase noise) and a 80 km fiber link (low dispersion scenario). The transmitted signal power is set as 5 dBm per channel, which is much higher than the optimal signal power. In this scenario the transmitted signal is distorted by the NLPN. BERs of the simulations with and without the application of MVV CPR are 8.1×10^{-4} and 1.6×10^{-3}, respectively. This indicates that MVV CPR could also mitigate the NLPN to a certain degree.

In addition, we extend the application of MVV CPR to the DP-256QAM transmission system and carry out numerical simulations to analyze the performance. The CPR length is set as 100. The green curve and the orange curve represent simulation results for the back-to-back and the 80 km transmission scenarios, respectively. We choose one point from each curve where the BER is approximately equal to

the target BER 4.5×10^{-3} and corresponding constellation diagrams are shown in the inset with green and orange colors. As shown in Fig. 9, MVV CPR can be applied to compensate for the laser phase noise in the DP-256QAM optical transmission scheme, especially with a moderate transmission distance, such as the data center systems. Since the 256QAM signal is much more sensitive to the laser phase noise and other distortions, e.g. EEPN, than the 64QAM signal, an obvious degradation in the performance of MVV CPR can be observed. It can be found from constellations in Fig. 10 that the laser phase noise in symbol points close to the center of the diagram could be efficiently eliminated, while the symbol points close to the edge of the constellations are still severely distorted.

5. Comparison with other CPR approaches

In this section, we compare by numerical simulations the proposed MVV algorithm with other CPR approaches, including Viterbi-Viterbi, rotation algorithm and constellation transformation, in terms of the performance and the computational complexity. To simplify the discussion, only key equations of the three algorithms are listed to analyze the complexity. The whole principles of VV, RA, and CT CPR approaches are described in [13,27,29] in detail.

5.1. Viterbi-Viterbi CPR

VV CPR [13], as the theoretical basis of MVV, RA, and CT algorithms, is originally designed for the QPSK modulation format. The core idea is to remove the data-modulated phase in the symbol by conducting the fourth power operation, in order to estimate the laser phase noise. However, the difference from the MVV method lies in the ring division step. For the application of VV in the 64QAM system [27], a ring division operation is also required at the first step and the fourth power operation is only applied to $Ring_1$, $Ring_3$, and $Ring_9$, as shown in Fig. 2. Namely, VV CPR only deals with symbols at $Ring_{QPSK}$ (into the fourth power) to cancel the phase modulation, and the rest of symbols are replaced with zeros. Then the estimated phase fluctuations (obtained from symbols at $Ring_{QPSK}$ only) are summed up and averaged over the entire CPR window. The extracted laser phase noise in the 64QAM coherent transmission system using the Viterbi–Viterbi method can be expressed as

$$\phi(n) = \frac{1}{4} angle \left\{ \sum_{k=-N}^{k=N} Y(n+k), Y(n+k) \in Ring_{QPSK} \right\} \quad (8)$$

where $\phi(n)$ represents the estimated laser phase noise of the nth symbol and $Ring_{QPSK}$ denotes $Ring_1$, $Ring_3$, and $Ring_9$ shown in Fig. 2.

5.2. Rotation algorithm CPR

RA CPR is an effective method to estimate the laser phase noise [26, 27]. Similar to MVV, RA CPR also divides the 64QAM constellation into 9 rings as shown in Fig. 2 and rotates symbols at $Ring_{rot}$. Nevertheless, there is significant difference between RA CPR and MVV CPR. On one hand, VV algorithm needs to be applied to provide a coarse phase estimation before the application of RA CPR. On the other hand, in the rotation step RA CPR firstly performs the fourth power operation on all rings and then utilizes the *signum* function to guarantee the proper rotations:

$$RA_y = C_y \cdot exp[4i\theta_x \cdot sgn(C_{yi})] \quad (9)$$

where C_y represents the symbol points on which the fourth power operations have been conducted, and $C_y i$ is the imaginary part of C_y. In other words, RA CPR employs the *signum* function to decide the direction of the rotation of the considered symbol and then carries out the proper rotation. By contrast, MVV CPR firstly rotates symbols at $Ring_{rot}$ either clockwise or anticlockwise, and then sets a threshold to exclude improperly rotated symbols.
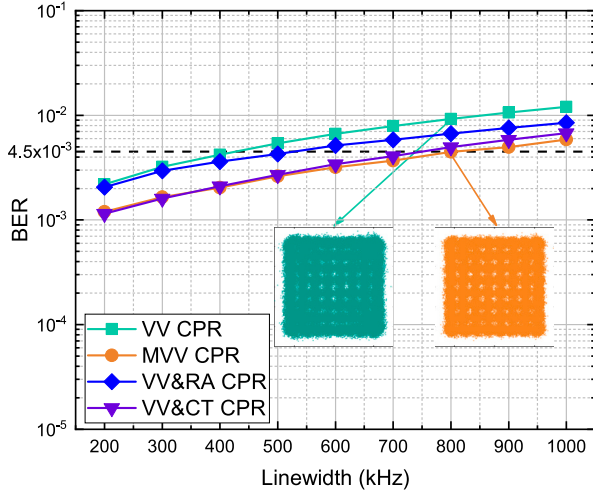
Fig. 10. BER versus laser linewidth in the transmission system of Fig. 3 with a modulation format of DP-64QAM and a transmission distance of 400 km, where VV, MVV, VV&RA, and VV&CT CPR have been applied respectively. The laser linewidth varies from 200 kHz to 1 MHz, and the length of transmitted symbol sequence is 2^{18}.

5.3. Constellation transformation CPR

The constellation transformation method is also an efficient carrier phase recovery algorithm [28,29]. The difference with regard to MVV CPR can be explained from two aspects. Firstly, a coarse pre-estimation using VV algorithm before the application of CT CPR is again required. Secondly, CT CPR aim to obtain a further fine estimation by splitting the 64QAM constellation down to QPSK cells rather than dividing all 64QAM symbols into 9 rings and performing rotations. For this purpose, the first step in CT CPR is to classify all symbol points into four groups, to achieve the 16QAM pairing based on the 64QAM constellation:

$$
\begin{aligned}
X = \ & Y_{1r} - sgn[Y_{1r} - 2sgn(Y_{1r})] \\
& + i\{Y_{1i} - sgn[Y_{1i} - 2sgn(Y_{1i})]\} \\
& + Y_{2r} - sgn[Y_{2r} - 2sgn(Y_{2r})] \\
& + i\{Y_{2i} - sgn[Y_{2i} - 6sgn(Y_{2i})]\} \\
& + Y_{3r} - sgn[Y_{3r} - 6sgn(Y_{3r})] \\
& + i\{Y_{3i} - sgn[Y_{3i} - 6sgn(Y_{3i})]\} \\
& + Y_{4r} - sgn[Y_{4r} - 6sgn(Y_{4r})) \\
& + i\{Y_{4i} - sgn[Y_{4i} - 2sgn(Y_{4i})]\}
\end{aligned}
\tag{10}
$$

where Y_{1r}, Y_{1i}, Y_{2r}, Y_{2i}, Y_{3r}, Y_{3i}, Y_{4r}, and Y_{4i} are the real and the imaginary parts of the four 16QAM pairing groups, respectively, and $sgn(\cdot)$ is the *signum* function. After that, symbols X in the obtained 16QAM constellation groups are further transformed to QPSK cells with the following operation

$$
\begin{aligned}
Z = \ & X_r - 2sgn[X_r - 4sgn(X_r)] \\
& + i\{X_i - 2sgn[X_i - 4sgn(X_i)]\}
\end{aligned}
\tag{11}
$$

where X_r and X_i denote the real and the imaginary parts of X, and Z represents the symbol in the ultimately-transformed QPSK cells, and $sgn(\cdot)$ is the *signum* function. After this, all processed symbols are raised to the power of four (to remove the data-modulated phase and) to estimate the laser phase noise [13–15].

5.4. Performance comparison

To comprehensively assess MVV, additional simulations have been carried out to compare the performance of MVV, VV, VV&RA, and VV&CT CPR. Results are illustrated in Fig. 10.

Table 2
Computational complexity per symbol in different CPR algorithms.

CPR	Complex multiplications (M) & Block update efforts (B)
VV	$\frac{16}{3}M + B$
MVV	$7M + B$
VV&RA	$\frac{37}{3}M + 2B$
VV&CT	$\frac{37}{3}M + 2B$

Green, orange, blue, and purple curves represent simulation results of VV, MVV, VV&RA, and VV&CT CPR, respectively. After a few tests, the optimum CPR length of VV, MVV, VV&RA, and VV&CT algorithms have been obtained as 121, 61, 121&51, and 121&21, respectively. It is noted that the optimum CPR lengths of VV&RA and VV&CT algorithms are not exactly the same as reported in [27,29], due to the difference in system parameters. At the linewidth of 800 kHz, constellation diagrams of signals processed after VV CPR and MVV CPR are listed in the inset with green and orange points, respectively. It is found in Fig. 10 that, MVV, VV&RA and VV&CT algorithms show better performance than VV CPR, and MVV CPR slightly outperforms VV&RA CPR while behaves similarly as VV&CT CPR.

5.5. Computational complexity

The computational complexity of VV, MVV, VV&RA, and VV&CT algorithms has also been assessed, in terms of the number of complex multiplications and the block update efforts spent for each processed symbol. According to [84], one complex multiplication requires three real multiplications. Accordingly, the *signum* function requires one third complex multiplication (one real multiplication), and the *modulus* function needs one complex multiplication. Based on these considerations, the complexity of these algorithms for each processed symbol in the data block has been estimated in Table 2, where M and B denote the computational complexity of one complex multiplication and one block update, respectively [85]. The process of block update involves a multidisciplinary approach, such as the implementation, type and design of hardware. More detailed and in-depth investigations will be carried out in our future work.

It is found in Table 2 that, the number of complex multiplications and the block update efforts for each processed symbol in both VV&RA and VV&CT CPR are higher than those in MVV CPR, due to the use of VV algorithm for the pre-processing in VV&RA and VV&CT CPR. Note that the complexity of the ring division operation in VV CPR is lower than that in MVV CPR and RA CPR because only $Ring_1$, $Ring_3$, and $Ring_9$ instead of all 9 rings, need to be specified in VV CPR. It can be seen from Table 2 and Fig. 10 that, compared to VV CPR, MVV CPR could achieve a better performance despite a slight increase of complexity. Compared to VV&RA and VV&CT CPR, MVV CPR could provide slightly better or similar performance, but with a lower complexity.

6. Discussions

Simulations have also been conducted to evaluate the efficacy of MVV CPR in the transmission system employing DP-1024QAM modulation. Results are depicted in Fig. 11. The illustration highlights the capability of MVV CPR in effectively mitigating the laser phase noise in a DP-1024QAM back-to-back system. Notably, the original signal exhibited a BER of 0.40, whereas the signal processed by MVV CPR reduced the BER significantly to 0.0013.

Besides, to further explore the efficacy of MVV CPR in a practical scenario, we have also conducted additional simulations and introduced practical distortions to the transmission system illustrated in
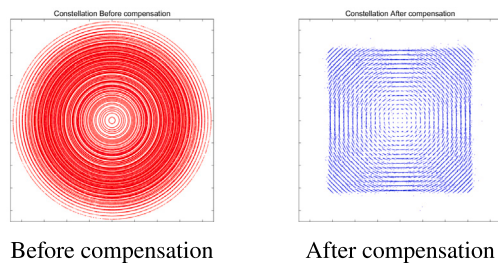
Before compensation   After compensation

Fig. 11. Simulated constellations in the back-to-back system for DP-1024QAM with linewidths of 100 kHz, where MVV CPR have been applied. The length of transmitted symbol sequence is 2^{19}.
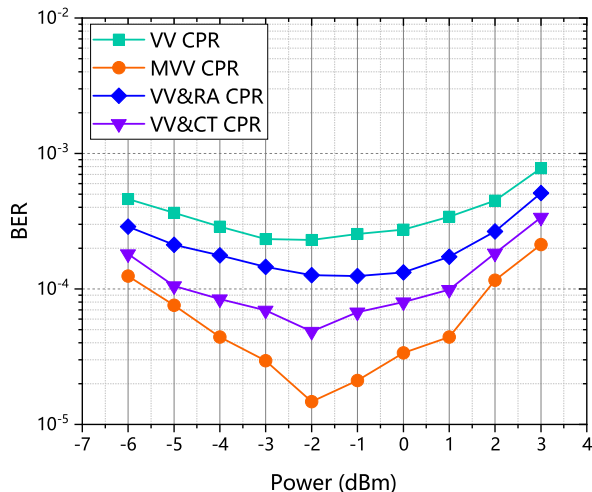

Fig. 12. Simulated curves of BER versus optical launch power per channel in the transmission system for DP-64QAM over a 80 km fiber link, where VV CPR, MVV CPR, VV&RA CPR, and VV&CT CPR have been applied respectively. The length of transmitted symbol sequence is 2^{18}.

Fig. 3. In this setup, the frequency offset between the transmitter and receiver lasers is set to 5 GHz, while the linewidths of both lasers are adjusted to 100 kHz [86,87]. Additionally, the roll-off of the root-raised cosine (RRC) filter is set as 1%. Simulation results are represented by green, orange, blue, and purple curves, corresponding to the VV, MVV, VV&RA, and VV&CT CPR techniques, respectively. The optimal CPR lengths for the VV, MVV, VV&RA, and VV&CT algorithms are determined as 121, 101, 121&101, and 121&101, respectively. The analysis depicted in Fig. 12 reveals that within this more realistic scenario, the MVV, VV&RA, and VV&CT algorithms exhibit superior performance compared to the VV CPR method. Furthermore, it is observed that MVV CPR consistently outperforms both VV&RA CPR and VV&CT CPR.

7. Conclusion

In this paper, we have developed an MVV CPR algorithm for the DP-64QAM coherent optical transmission system and have carried out comprehensive numerical simulations to analyze the performance of MVV CPR. With a reference of PA CPR, we have investigated the performance of MVV CPR in the back-to-back system and the transmission system with a 400 km fiber link. Results indicate that MVV CPR could greatly suppress the laser phase noise. Then we have compared the performance of MVV CPR and PA CPR in the nonlinear optical transmission systems with different transmission distances and laser linewidths. It is found that, compared to PA CPR, MVV CPR performs better when the transmission distance increases because of the capability in mitigating the influence of EEPN due to the averaging function of the sliding

window. For a linewidth of 100 kHz, the maximum reach of the DP-64QAM transmission system using MVV CPR is around 600 km at the target BER of 4.5×10^{-3}. Meanwhile, it is found that MVV CPR can also be applied in the DP-256QAM optical transmission systems. In addition, MVV CPR is also compared to another three CPR approaches, including VV, VV&RA and VV&CT algorithms, in terms of performance and computational complexity.

Our work demonstrates the feasibility of upgrading the conventional VV algorithm (based on QPSK partitioning) in next-generation optical communications, when current commercial DP-16QAM 200 Gbit/s/λ optical transmission systems are further promoted with higher-order modulation formats, higher symbol rate, wider bandwidth, and narrower channel spacing, where more significant EEPN and fiber nonlinearities have to be considered. This work not only shows the application and the performance of the updated MVV algorithm in such optical communication systems, but also provides comprehensive insights and in-depth visions in the upgrade and the evaluation of other popular CPR algorithms.

CRediT authorship contribution statement

Yunfan Zhang: Writing – original draft, Investigation. **Tiegen Liu:** Supervision, Resources, Formal analysis. **Cenqin Jin:** Software, Formal analysis. **Tongyang Xu:** Formal analysis. **Mingming Tan:** Formal analysis. **Jian Zhao:** Supervision, Formal analysis. **Tianhua Xu:** Writing – review & editing, Software, Investigation, Formal analysis.

Declaration of competing interest

The authors declare that they have no known competing financial interests or personal relationships that could have appeared to influence the work reported in this paper.

Data availability

Data will be made available on request.

References

[1] T. Xu, N.A. Shevchenko, Y. Zhang, C. Jin, J. Zhao, T. Liu, Information rates in Kerr nonlinearity limited optical fiber communication systems, Opt. Express 29 (11) (2021) 17428–17439.

[2] J. Yang, E. Sillekens, W. Yi, P. Bayvel, R.I. Killey, Joint estimation of dynamic polarization and carrier phase with pilot-based adaptive equalizer in PDM-64 QAM transmission system, Opt. Express 29 (26) (2021) 43136–43147, http://dx.doi.org/10.1364/OE.445400, URL https://hfcba7887ad1d28f444b4hbpqffu0uq5cx6pbcfbhy.eds.tju.edu.cn/oe/abstract.cfm?URI=oe-29-26-43136.

[3] G. Bosco, A. Carena, V. Curri, P. Poggiolini, F. Forghieri, Performance limits of Nyquist-WDM and CO-OFDM in high-speed PM-QPSK systems, IEEE Photonics Technol. Lett. 22 (15) (2010) 1129–1131, http://dx.doi.org/10.1109/LPT.2010.2050581.

[4] C.E. Shannon, A mathematical theory of communication, Bell Syst. Tech. J. 27 (3) (1948) 379–423.

[5] C. Jin, N.A. Shevchenko, Z. Li, S. Popov, Y. Chen, T. Xu, Nonlinear coherent optical systems in the presence of equalization enhanced phase noise, J. Lightwave Technol. 39 (14) (2021) 4646–4653, http://dx.doi.org/10.1109/JLT.2021.3076067.

[6] T. Xu, G. Liga, D. Lavery, B.C. Thomsen, S.J. Savory, R.I. Killey, P. Bayvel, Equalization enhanced phase noise in nyquist-spaced superchannel transmission systems using multi-channel digital back-propagation, Sci. Rep. 5 (1) (2015) 13990.

[7] A. Kakkar, J.R. Navarro, R. Schatz, H. Louchet, X. Pang, O. Ozolins, G. Jacobsen, S. Popov, Comprehensive study of equalization-enhanced phase noise in coherent optical systems, J. Lightwave Technol. 33 (23) (2015) 4834–4841.

[8] A. Kakkar, J. Rodrigo Navarro, R. Schatz, X. Pang, O. Ozolins, A. Udalcovs, H. Louchet, S. Popov, G. Jacobsen, Laser frequency noise in coherent optical systems: spectral regimes and impairments, Sci. Rep. 7 (1) (2017) 844.

[9] A. Kakkar, R. Schatz, X. Pang, J.R. Navarro, H. Louchet, O. Ozolins, G. Jacobsen, S. Popov, Impact of local oscillator frequency noise on coherent optical systems with electronic dispersion compensation, Opt. Express 23 (9) (2015) 11221–11226.

[10] T. Inoue, S. Namiki, Carrier recovery for M-QAM signals based on a block estimation process with Kalman filter, Opt. Express 22 (13) (2014) 15376–15387, http://dx.doi.org/10.1364/OE.22.015376, URL https://hfcba7887ad1d28f444b4hbpqffu0uq5cx6pbcfbhy.eds.tju.edu.cn/oe/abstract.cfm?URI=oe-22-13-15376.

[11] J.C.M. Diniz, Q. Fan, S.M. Ranzini, F.N. Khan, F.D. Ros, D. Zibar, A.P.T. Lau, Low-complexity carrier phase recovery based on principal component analysis for square-QAM modulation formats, Opt. Express 27 (11) (2019) 15617–15626, http://dx.doi.org/10.1364/OE.27.015617, URL https://hfcba7887ad1d28f444b4hbpqffu0uq5cx6pbcfbhy.eds.tju.edu.cn/oe/abstract.cfm?URI=oe-27-11-15617.

[12] S.M. Bilal, K.P. Zhong, J. Cheng, A.P.T. Lau, G. Bosco, C. Lu, Performance and complexity comparison of carrier phase estimation algorithms for DP-64-QAM optical signals, in: 2014 the European Conference on Optical Communication, ECOC, 2014, pp. 1–3, http://dx.doi.org/10.1109/ECOC.2014.6964034.

[13] A.J. Viterbi, A.M. Viterbi, Nonlinear estimation of PSK-modulated carrier phase with application to burst digital transmission, IEEE T. Inform. Theory 29 (4) (1983) 543–551, http://dx.doi.org/10.1109/TIT.1983.1056713.

[14] S.O. Zafra, X. Pang, G. Jacobsen, S. Popov, S. Sergeyev, Phase noise tolerance study in coherent optical circular QAM transmissions with viterbi-viterbi carrier phase estimation, Opt. Express 22 (25) (2014) 30579–30585.

[15] Y. Li, M.-W. Wu, X. Du, T. Song, P.-Y. Kam, A refinement to the viterbi-viterbi carrier phase estimator and an extension to the case with a Wiener carrier phase process, IEEE Access 7 (2019) 78170–78184, http://dx.doi.org/10.1109/ACCESS.2019.2922313.

[16] F. Rice, B. Cowley, B. Moran, M. Rice, Cramer-rao lower bounds for QAM phase and frequency estimation, IEEE Trans. Commun. 49 (9) (2001) 1582–1591, http://dx.doi.org/10.1109/26.950345.

[17] S. Oh, S. Stapleton, Blind phase recovery using finite alphabet properties in digital communications, Electron. Lett. 33 (3) (1997) 175–176.

[18] T. Pfau, S. Hoffmann, R. Noé, Hardware-efficient coherent digital receiver concept with feedforward carrier recovery for *M*-QAM constellations, J. Lightwave Technol. 27 (8) (2009) 989–999.

[19] G. di Rosa, A. Richter, Achievable mitigation of nonlinear phase noise through optimized blind carrier phase recovery, in: 2020 22nd International Conference on Transparent Optical Networks, ICTON, 2020, pp. 1–4, http://dx.doi.org/10.1109/ICTON51198.2020.9203148.

[20] Z. Chen, S. Fu, M. Tang, Z. Zhang, Y. Qin, Maximum probability directed blind phase search for PS-QAM with variable shaping factors, Opt. Express 30 (1) (2022) 550–562, http://dx.doi.org/10.1364/OE.448613, URL https://hfcba7887ad1d28f444b4hbpqffu0uq5cx6pbcfbhy.eds.tju.edu.cn/oe/abstract.cfm?URI=oe-30-1-550.

[21] I. Fatadin, D. Ives, S.J. Savory, Laser linewidth tolerance for 16-QAM coherent optical systems using QPSK partitioning, IEEE Photonic Tech. L. 22 (9) (2010) 631–633.

[22] I. Fatadin, D. Ives, S.J. Savory, Carrier phase recovery for 16-QAM using QPSK partitioning and sliding window averaging, IEEE Photonic Tech. L. 26 (9) (2014) 854–857, http://dx.doi.org/10.1109/LPT.2014.2306001.

[23] H. Tang, S. Fu, H. Liu, M. Tang, P. Shum, D. Liu, Low-complexity carrier phase recovery based on constellation classification for M-ary offset-QAM signal, J. Lightwave Technol. 34 (4) (2016) 1133–1140, http://dx.doi.org/10.1109/JLT.2016.2515618.

[24] K. Shibahara, T. Mizuno, Y. Miyamoto, MIMO carrier phase recovery for carrier-asynchronous SDM-MIMO reception based on the extended Kalman filter, Opt. Express 29 (11) (2021) 17111–17124, http://dx.doi.org/10.1364/OE.424235, URL https://hfcba7887ad1d28f444b4hbpqffu0uq5cx6pbcfbhy.eds.tju.edu.cn/oe/abstract.cfm?URI=oe-29-11-17111.

[25] L. Lundberg, B.J. Puttnam, R.S. Luís, G. Rademacher, M. Karlsson, P.A. Andrekson, Y. Awaji, N. Wada, Master-slave carrier recovery for M-QAM multicore fiber transmission, Opt. Express 27 (16) (2019) 22226–22236, http://dx.doi.org/10.1364/OE.27.022226, URL https://hfcba7887ad1d28f444b4hbpqffu0uq5cx6pbcfbhy.eds.tju.edu.cn/oe/abstract.cfm?URI=oe-27-16-22226.

[26] K.P. Zhong, J.H. Ke, Y. Gao, J.C. Cartledge, Linewidth-tolerant and low-complexity two-stage carrier phase estimation based on modified QPSK partitioning for dual-polarization 16-QAM systems, J. Lightwave Technol. 31 (1) (2013) 50–57, http://dx.doi.org/10.1109/JLT.2012.2227457.

[27] S.M. Bilal, G. Bosco, J. Cheng, A.P.T. Lau, C. Lu, Carrier phase estimation through the rotation algorithm for 64-QAM optical systems, J. Lightwave Technol. 33 (9) (2015) 1766–1773, http://dx.doi.org/10.1109/JLT.2015.2402441.

[28] J.H. Ke, K.P. Zhong, Y. Gao, J.C. Cartledge, A.S. Karar, M.A. Rezania, Linewidth-tolerant and low-complexity two-stage carrier phase estimation for dual-polarization 16-QAM coherent optical fiber communications, J. Lightwave Technol. 30 (24) (2012) 3987–3992, http://dx.doi.org/10.1109/JLT.2012.2208448.

[29] S.M. Bilal, C.R.S. Fludger, V. Curri, G. Bosco, Multistage carrier phase estimation algorithms for phase noise mitigation in 64-quadrature amplitude modulation optical systems, J. Lightwave Technol. 32 (17) (2014) 2973–2980, http://dx.doi.org/10.1109/JLT.2014.2325064.

[30] M. Nakamura, Y. Kamio, T. Miyazaki, Linewidth-tolerant 10-gbit/s 16-QAM transmission using a pilot-carrier based phase-noise cancelling technique, Opt. Express 16 (14) (2008) 10611–10616, http://dx.doi.org/10.1364/OE.16.010611, URL https://ifcba7887ad1d28f444b4h05fvkf6ox0x56kcvfbhy.eds.tju.edu.cn/oe/abstract.cfm?URI=oe-16-14-10611.

[31] M. Nakamura, Y. Kamio, T. Miyazaki, Pilot-carrier based linewidth-tolerant 8PSK self-homodyne using only one modulator, in: 33rd European Conference and Exhibition of Optical Communication, VDE, 2007, pp. 1–2.

[32] G. Jacobsen, T. Xu, S. Popov, J. Li, A.T. Friberg, Y. Zhang, Receiver implemented RF pilot tone phase noise mitigation in coherent optical nPSK and nQAM systems, Opt. Express 19 (15) (2011) 14487–14494.

[33] J. Yang, E. Sillekens, W. Yi, P. Bayvel, R.I. Killey, Joint estimation of dynamic polarization and carrier phase with pilot-based adaptive equalizer in PDM-64 QAM transmission system, Opt. Express 29 (26) (2021) 43136–43147, http://dx.doi.org/10.1364/OE.445400, URL https://ifcba7887ad1d28f444b4h05fvkf6ox0x56kcvfbhy.eds.tju.edu.cn/oe/abstract.cfm?URI=oe-29-26-43136.

[34] T. Xu, G. Jacobsen, S. Popov, J. Li, A.T. Friberg, Y. Zhang, Phase noise mitigation in coherent transmission system using a pilot carrier, in: 2011 Asia Communications and Photonics Conference and Exhibition, ACP, 2011, pp. 1–6, http://dx.doi.org/10.1117/12.904038.

[35] Y. Takanashi, S. Owaki, R. Nakamura, M. Nakamura, SPM and phase-noise compensation using a time-division-multiplexed and intensity modulated pilot-carrier, in: 2017 Opto-Electronics and Communications Conference (OECC) and Photonics Global Conference, PGC, 2017, pp. 1–2, http://dx.doi.org/10.1109/OECC.2017.8114899.

[36] M. Morsy-Osman, Q. Zhuge, L.R. Chen, D.V. Plant, Feedforward carrier recovery via pilot-aided transmission for single-carrier systems with arbitrary M-QAM constellations, Opt. Express 19 (24) (2011) 24331–24343, http://dx.doi.org/10.1364/OE.19.024331, URL http://opg.optica.org/oe/abstract.cfm?URI=oe-19-24-24331.

[37] F. Zhang, Y. Li, J. Wu, W. Li, X. Hong, J. Lin, Improved pilot-aided optical carrier phase recovery for coherent *M*-QAM, IEEE Photonics Lett. 24 (18) (2012) 1577–1580, http://dx.doi.org/10.1109/LPT.2012.2208739.

[38] J. Lin, Z. Zhang, L. Xi, X. Zhang, Pilot-tone-aided two-stage carrier phase recovery in dual-carrier nyquist m-QAM transmission system, in: 2014 Conference on Lasers and Electro-Optics (CLEO) - Laser Science To Photonic Applications, 2014, pp. 1–2.

[39] M.A. Castrillón, D.A. Morero, M.R. Hueda, Carrier phase recovery without pilot symbols for non-differential coherent receivers, in: Optical Fiber Communication Conference, Optica Publishing Group, 2016, p. Tu3K.4, http://dx.doi.org/10.1364/OFC.2016.Tu3K.4, URL http://opg.optica.org/abstract.cfm?URI=OFC-2016-Tu3K.4.

[40] H. Cui, X. Xu, S. Liu, Y. Lu, Y. Qiao, QPSK pilot-aided carrier phase recovery algorithm for 800-gb/s/λ DP-256QAM transmission, in: Asia Communications and Photonics Conference/International Conference on Information Photonics and Optical Communications 2020 (ACP/IPOC), Optica Publishing Group, 2020, p. M4A.217, http://dx.doi.org/10.1364/ACPC.2020.M4A.217, URL http://opg.optica.org/abstract.cfm?URI=ACPC-2020-M4A.217.

[41] S.M. Bilal, G. Bosco, Pilot tones based polarization rotation, frequency offset and phase estimation for polarization multiplexed offset-QAM multi-subcarrier coherent optical systems, in: 2016 18th International Conference on Transparent Optical Networks, ICTON, 2016, pp. 1–4, http://dx.doi.org/10.1109/ICTON.2016.7550259.

[42] X. Yan, C. Cao, W. Zhang, X. Zeng, Z. Feng, Z. Wu, X. Su, T. Wang, Low-complexity carrier phase estimation for M-ary quadrature amplitude modulation optical communication based on dichotomy, Opt. Express 28 (17) (2020) 25263–25277.

[43] T. Yang, C. Shi, X. Chen, M. Zhang, Y. Ji, F. Hua, Y. Chen, Linewidth-tolerant and multi-format carrier phase estimation schemes for coherent optical m-QAM flexible transmission systems, Opt. Express 26 (8) (2018) 10599–10615, http://dx.doi.org/10.1364/OE.26.010599, URL http://www.opticsexpress.org/abstract.cfm?URI=oe-26-8-10599.

[44] Y. Li, T. Song, M. Gurusamy, C. Yu, P.-Y. Kam, Enhanced adaptive DA-ML carrier phase estimator and its application to accurate laser linewidth and SNR estimation, Opt. Express 26 (12) (2018) 14817–14831.

[45] C.S. Martins, A. Lorences-Riesgo, M.S. Neves, S. Mumtaz, Y. Frignac, T.H. Nguyen, P.P. Monteiro, G. Charlet, F.P. Guiomar, S. Dris, Maximizing the performance of digital multi-carrier systems with transmission-aware joint carrier phase recovery, in: 2021 European Conference on Optical Communication, ECOC, 2021, pp. 1–4, http://dx.doi.org/10.1109/ECOC52684.2021.9606142.

[46] Y. Zhang, T. Xu, J. Ding, Z. Wang, T. Xu, J. Zhao, T. Liu, Carrier phase recovery in optical fiber communication systems using high-order modulation formats, in: Semiconductor Lasers and Applications XI, SPIE, 11891, 2021, pp. 14–23.

[47] T. Sasai, A. Matsushita, M. Nakamura, S. Okamoto, F. Hamaoka, Y. Kisaka, Laser phase noise tolerance of uniform and probabilistically shaped QAM signals for high spectral efficiency systems, J. Lightwave Technol. 38 (2) (2019) 439–446.

[48] J. Kahn, L. Kazovsky, Coherent optical communications: Fundamentals and future prospects, Front. Opt. (2006) FThI1, http://dx.doi.org/10.1364/FIO.2006.FThI1, URL http://opg.optica.org/abstract.cfm?URI=FiO-2006-FThI1.

[49] K. Kikuchi, Characterization of semiconductor-laser phase noise and estimation of bit-error rate performance with low-speed offline digital coherent receivers, Opt. Express 20 (5) (2012) 5291–5302, http://dx.doi.org/10.1364/OE.20.005291, URL http://www.opticsexpress.org/abstract.cfm?URI=oe-20-5-5291.

[50] R. Noé, Phase noise-tolerant synchronous QPSK/BPSK baseband-type intradyne receiver concept with feedforward carrier recovery, J. Lightwave Technol. 23 (2) (2005) 802–808.

[51] Y. Li, Q. Zheng, Y. Xie, J. Han, W. Li, Low complexity carrier phase estimation for m-QAM optical communication systems, Photonic Netw. Commun. 38 (1) (2019) 121–128.

[52] J.R. Navarro, A. Kakkar, X. Pang, O. Ozolins, R. Schatz, M.I. Olmedo, G. Jacobsen, S. Popov, Carrier phase recovery algorithms for coherent optical circular mQAM systems, J. Lightwave Technol. 34 (11) (2016) 2717–2723.

[53] E. Ip, J.M. Kahn, Feedforward carrier recovery for coherent optical communications, J. Lightwave Technol. 25 (9) (2007) 2675–2692.

[54] X. Fang, F. Zhang, Phase noise estimation and suppression for PDM CO-OFDM/OQAM systems, J. Lightwave Technol. 35 (10) (2017) 1837–1846, URL http://jlt.osa.org/abstract.cfm?URI=jlt-35-10-1837.

[55] D. Lippiatt, S. Varughese, T. Richter, S. Tibuleac, S.E. Ralph, Joint linear and nonlinear noise estimation of optical links by exploiting carrier phase recovery, 2020, p. Th2A.49, http://dx.doi.org/10.1364/OFC.2020.Th2A.49, URL http://opg.optica.org/abstract.cfm?URI=OFC-2020-Th2A.49,

[56] T.T. Nguyen, S. Boscolo, A. Ali, M. Tan, T. Zhang, S. Takasaka, R. Sugizaki, S. Sygletos, A.D. Ellis, Kernel-based learning-aided phase noise compensation in dual-pump optical phase conjugation coherent system, in: 2021 Optical Fiber Communications Conference and Exhibition, OFC, 2021, pp. 1–3.

[57] F.K. Deynu, E.W. Akpari, C. Akama, Phase noise effects on the performance of joint carrier phase recovery algorithms in phase-locked WDM superchannel transmission systems, Opt. Fiber Technol., Mater. Devices Syst. 54 (2020) 102104.

[58] S.-Y. Kim, T. Suzuki, J.-I. Kani, T. Yoshida, Carrier phase estimation softwarized on GPU using decision-aided phase unwrapping for flexible optical coherent access systems, J. Lightwave Technol. 39 (6) (2021) 1706–1714, URL http://jlt.osa.org/abstract.cfm?URI=jlt-39-6-1706.

[59] C. Li, D. Pan, Y. Feng, J. Lin, L. Xi, X. Tang, W. Zhang, X. Zhang, Carrier phase estimation scheme for faster-than-nyquist optical coherent communication systems, Chin. Opt. Lett. 14 (10) (2016) 100601, URL http://col.osa.org/abstract.cfm?URI=col-14-10-100601.

[60] M.S. Neves, P.P. Monteiro, F.P. Guiomar, Enhanced phase estimation for long-haul multi-carrier systems using a dual-reference subcarrier approach, J. Lightwave Technol. 39 (9) (2021) 2714–2724, URL http://jlt.osa.org/abstract.cfm?URI=jlt-39-9-2714.

[61] K. Zhong, J.H. Ke, Y. Gao, J.C. Cartledge, Linewidth-tolerant and low-complexity two-stage carrier phase estimation based on modified QPSK partitioning for dual-polarization 16-QAM systems, J. Lightwave Technol. 31 (1) (2013) 50–57, URL http://jlt.osa.org/abstract.cfm?URI=jlt-31-1-50.

[62] I. Fatadin, D. Ives, S.J. Savory, Carrier phase recovery for 16-QAM using QPSK partitioning and sliding window averaging, IEEE Photonics Technol. Lett. 26 (9) (2014) 854–857, http://dx.doi.org/10.1109/LPT.2014.2306001.

[63] D.-S. Ly-Gagnon, S. Tsukamoto, K. Katoh, K. Kikuchi, Coherent detection of optical quadrature phase-shift keying signals with carrier phase estimation, J. Lightwave Technol. 24 (1) (2006) 12, URL http://opg.optica.org/jlt/abstract.cfm?URI=jlt-24-1-12.

[64] Y. Wang, Z. Wu, X. Li, T. Geng, S. Ma, L. Li, S. Gao, Y. Li, Non-data-aided cycle slip self-correcting carrier phase estimation for QPSK modulation format of coherent wireless optical communication system, IEEE Access 7 (2019) 110451–110462, http://dx.doi.org/10.1109/ACCESS.2019.2934224.

[65] Y. Gao, E. Ha, A.P.T. Lau, C. Lu, X. Xu, L. Li, Non-data-aided and universal cycle slip detection and correction for coherent communication systems, Opt. Express 22 (25) (2014) 31167–31179, http://dx.doi.org/10.1364/OE.22.031167, URL https://ifcba7887ad1d28f444b4h0x55wfpwqnvb69pcfbhy.eds.tju.edu.cn/oe/abstract.cfm?URI=oe-22-25-31167.

[66] S.-Y. Kim, T. Suzuki, J.-I. Kani, T. Yoshida, Carrier phase estimation softwarized on GPU using decision-aided phase unwrapping for flexible optical coherent access systems, J. Lightwave Technol. 39 (6) (2021) 1706–1714, URL https://ifcba7887ad1d28f444b4h0x55wfpwqnvb69pcfbhy.eds.tju.edu.cn/jlt/abstract.cfm?URI=jlt-39-6-1706.

[67] T. Xu, G. Jacobsen, S. Popov, J. Li, E. Vanin, K. Wang, A.T. Friberg, Y. Zhang, Chromatic dispersion compensation in coherent transmission system using digital filters, Opt. Expr. 18 (15) (2010) 16243–16257.

[68] W. Lalu, B. Alvarez, C.D. Cruz, L. Lauan, J. Trinos, R.A. Yanza, C.H. Weng, G. Tan, J.D. Cruz, Carrier phase recovery estimation algorithms in optical coherent QPSK communication system, in: 2021 International Conference on Smart Generation Computing, Communication and Networking, SMART GENCON, 2021, pp. 1–6, http://dx.doi.org/10.1109/SMARTGENCON51891.2021.9645800.

[69] Z. Song, K. Igarashi, Achievable information rate performance comparison of frequency-pilot-aided and blind carrier phase estimation methods, in: 2020 Asia Communications and Photonics Conference (ACP) and International Conference on Information Photonics and Optical Communications, IPOC, 2020, pp. 1–3.

[70] A. Bisplinghoff, C. Fludger, T. Kupfer, B. Schmauss, Carrier and phase recovery algorithms for QAM constellations: Real-time implementations, in: Advanced Photonics 2013, Optica Publishing Group, 2013, p. SPM4D.1, http://dx.doi.org/10.1364/SPPCOM.2013.SPM4D.1, URL https://ifcba7887ad1d28f444b4h5fvq0copkf95695nfbhy.eds.tju.edu.cn/abstract.cfm?URI=SPPCom-2013-SPM4D.1.

[71] J. Liu, Improved carrier phase estimation algorithms for optical coherent systems, in: 2012 2nd International Conference on Consumer Electronics, Communications and Networks, CECNet, 2012, pp. 1845–1847, http://dx.doi.org/10.1109/CECNet.2012.6201813.

[72] Y. Gao, A.P.T. Lau, S. Yan, C. Lu, Low-complexity and phase noise tolerant carrier phase estimation for dual-polarization 16-QAM systems, Opt. Express 19 (22) (2011) 21717–21729.

[73] C. Xie, Local oscillator phase noise induced penalties in optical coherent detection systems using electronic chromatic dispersion compensation, in: 2009 Conference on Optical Fiber Communication, OFC, 2009, pp. 1–3.

[74] W. Shieh, K.-P. Ho, Equalization-enhanced phase noise for coherent-detection systems using electronic digital signal processing, Opt. Express 16 (20) (2008) 15718–15727, http://dx.doi.org/10.1364/OE.16.015718, URL https://hfcba7887ad1d28f444b4h990qnpkvo6u96woxfbhy.eds.tju.edu.cn/oe/abstract.cfm?URI=oe-16-20-15718.

[75] A.P.T. Lau, T.S.R. Shen, W. Shieh, K.-P. Ho, Equalization-enhanced phase noise for 100gb/s transmission and beyond with coherent detection, Opt. Express 18 (16) (2010) 17239–17251, http://dx.doi.org/10.1364/OE.18.017239, URL https://hfcba7887ad1d28f444b4hbb9nnv0xw9u66knufbhy.eds.tju.edu.cn/oe/abstract.cfm?URI=oe-18-16-17239.

[76] M. Zhu, J. Zhang, X. Huang, X. Yi, B. Xu, K. Qiu, Influence of EEPN and P2A noise with CD pre- and post-compensation in optical SSB transmission and Kramers-Kronig receiver system, Opt. Express 27 (14) (2019) 19664–19674, http://dx.doi.org/10.1364/OE.27.019664, URL https://hfcba7887ad1d28f444b4hbb9nnv0xw9u66knufbhy.eds.tju.edu.cn/oe/abstract.cfm?URI=oe-27-14-19664.

[77] K. Saito, M. Nakamura, T. Sasai, T. Kakizaki, F. Hamaoka, T. Kobayashi, E. Yamazaki, Y. Kisaka, Impact of local oscillator phase noise on long-haul transmission of 120-gbaud digital sub-carrier signals, in: 2022 Optical Fiber Communications Conference and Exhibition, OFC, 2022, pp. 1–3.

[78] P. Qin, C. Bai, H. Xu, L. Yang, W. Sun, X. Yu, X. Lv, X. Tang, Y. Bi, X. Luo, Analysis and compensation of equalization-enhanced phase noise in carrier assisted differential detection system, in: 2021 Asia Communications and Photonics Conference, ACP, 2021, pp. 1–3.

[79] F. Pittalà, I.N. Cano, C. Bluemm, M. Schaedler, S. Calabrò, G. Goeger, R. Brenot, C. Xie, C. Shi, G.N. Liu, G. Charlet, M. Kuschnerov, 400-Gbit/s DP-16-QAM transmission over 40-km unamplified SSMF with low-cost PON lasers, IEEE Photonic Tech. L. 31 (15) (2019) 1229–1232, http://dx.doi.org/10.1109/LPT.2019.2922874.

[80] F. Chang, K. Onohara, T. Mizuochi, Forward error correction for 100 g transport networks, IEEE Commun. Mag. 48 (3) (2010) S48–S55, http://dx.doi.org/10.1109/MCOM.2010.5434378.

[81] Y. Pang, Y. Xu, X. Zhao, Z. Qin, Z. Liu, Stabilized narrow-linewidth brillouin random fiber laser with a double-coupler fiber ring resonator, J. Lightwave Technol. (2022 in press) http://dx.doi.org/10.1109/JLT.2022.3148118.

[82] A. Demir, Nonlinear phase noise in optical-fiber-communication systems, J. Lightwave Technol. 25 (8) (2007) 2002–2032, http://dx.doi.org/10.1109/JLT.2007.900888.

[83] O. Golani, D. Pilori, F.P.P. Guiomar, G. Bosco, A. Carena, M. Shtaif, Correlated nonlinear phase-noise in multi-subcarrier systems: Modeling and mitigation, J. Lightwave Technol. 38 (6) (2020) 1148–1156, http://dx.doi.org/10.1109/JLT.2019.2939706.

[84] Y. Mahdy, S. Ali, K. Shaaban, Algorithm and two efficient implementations for complex multiplier, in: ICECS'99. Proceedings of ICECS '99. 6th IEEE International Conference on Electronics, Circuits and Systems (Cat. No.99EX357), vol. 2, 1999, pp. 949–952, http://dx.doi.org/10.1109/ICECS.1999.813389.

[85] T. Xu, G. Jacobsen, S. Popov, J. Li, A.T. Friberg, Y. Zhang, Carrier phase estimation methods in coherent transmission systems influenced by equalization enhanced phase noise, Opt. Commun. 293 (2013) 54–60.

[86] L. Li, Z. Tao, S. Oda, T. Hoshida, J.C. Rasmussen, Wide-range, accurate and simple digital frequency offset compensator for optical coherent receivers, in: OFC/NFOEC 2008-2008 Conference on Optical Fiber Communication/National Fiber Optic Engineers Conference, IEEE, 2008, pp. 1–3.

[87] Optical Internetworking Forum, Integrable tunable laser assembly multi source agreement, 2015, https://www.oiforum.com/wp-content/uploads/2019/01/OIF-ITLA-MSA-01.3.pdf.